© 2015. Published by The Company of Biologists Ltd | Journal of Cell Science (2015) 128, 2351-2362 doi:10.1242/jcs.168740

RESEARCH ARTICLE

Architectures of multisubunit complexes revealed by a visible immunoprecipitation assay using fluorescent fusion proteins

Yohei Katoh*, Shohei Nozaki*, David Hartanto, Rie Miyano and Kazuhisa Nakayama‡

ABSTRACT

In this study, we elucidated the architectures of two multisubunit complexes, the BBSome and exocyst, through a novel application of fluorescent fusion proteins. By processing lysates from cells co-expressing GFP and RFP fusion proteins for immunoprecipitation with anti-GFP nanobody, protein–protein interactions could be reproducibly visualized by directly observing the immunoprecipitates under a microscope, and evaluated using a microplate reader, without requiring immunoblotting. Using this 'visible' immunoprecipitation (VIP) assay, we mapped binary subunit interactions of the BBSome complex, and determined the hierarchies of up to four subunit interactions. We also demonstrated the assembly sequence of the BBSome around the centrosome, and showed that BBS18 (also known as BBIP1 and BBIP10) serves as a linker between BBS4 and BBS8 (also known as TTC8). We also applied the VIP assay to mapping subunit interactions of the exocyst tethering complex. By individually subtracting the eight exocyst subunits from multisubunit interaction assays, we unequivocally demonstrated one-to-many subunit interactions (Exo70 with Sec10+Sec15, and Exo84 with Sec10+Sec15+Exo70). The simple, versatile VIP assay described here will pave the way to understanding the architectures and functions of multisubunit complexes involved in a variety of cellular processes.

KEY WORDS: Fluorescent fusion protein, Membrane traffic, Exocyst, BBSome, Protein–protein interaction, Anti-GFP nanobody

INTRODUCTION

Following the complete sequencing of the genomes of humans and other organisms, studies of the interactions between known proteins have improved our understanding of protein function. Protein–protein interactions can be assessed by a variety of methods. For example, pulldown assays using glutathione *S*-transferase (GST)-fusion proteins to precipitate cellular proteins, which are often exogenously expressed as epitope-tagged proteins, have often been employed to study protein–protein interactions *in vitro*; likewise, co-immunoprecipitation assays using antibodies to short epitope sequences to precipitate exogenously expressed epitope-tagged proteins have been used for a similar purpose in cells. In both types of assays, proteins interacting with the 'bait' proteins are usually detected by immunoblotting, which entails electrophoresis and subsequent electroblotting onto membranes, followed by detection with primary and secondary antibodies and chemiluminescence reagents. In addition, genetic methods, such as the yeast two-hybrid system, have also been frequently employed to reveal protein–protein interactions. However, two-hybrid assays have often yielded false-positive results and missed significant interactions (for example, see supplementary material Fig. S1), although they are higher in sensitivity and throughput than pulldown and co-immunoprecipitation assays.

Our group has been studying the regulation of intracellular protein trafficking by the membrane trafficking machineries. Various multisubunit complexes participate in membrane trafficking processes, including tethering and fusion of carrier vesicles with target membranes (Hong and Lev, 2014). For example, we have recently shown that the exocyst complex regulates tethering of transferrin-receptor-containing recycling vesicles to the plasma membrane, downstream of the Rab11 small GTPase (Takahashi et al., 2012). The exocyst is composed of eight subunits (Sec3, Sec5, Sec6, Sec8, Sec10, Sec15, Exo70, and Exo84 in yeast, and also known as EXOC1–EXOC8 in mammals) (Hsu et al., 1998; Terbush et al., 2001). However, the architecture of the complex is poorly understood (Liu and Guo, 2012; Munson and Novick, 2006).

Protein trafficking to and/or within cilia is also mediated by multisubunit complexes, including the BBSome, and intraflagellar transport (IFT)-A and IFT-B complexes (Sung and Leroux, 2013). The BBSome is composed of seven or eight subunits [BBS1, BBS2, BBS4, BBS5, BBS7, BBS8 (also known as TTC8), BBS9 and BBS18 (also known as BBIP1 and BBIP10)] and has been implicated in protein transport to and/or within the cilia (Jin and Nachury, 2009; Loktev et al., 2008; Sung and Leroux, 2013). All the BBS proteins were identified by mutations of their respective genes in patients with Bardet–Biedl syndrome (BBS), a genetically heterogeneous disease (ciliopathy) characterized by a wide spectrum of clinical features, including rod–cone dystrophy, morbid obesity, polydactyly, genital anomalies, learning difficulties, and renal anomalies (M'Hamdi et al., 2014; Madhivanan and Aguilar, 2014).

In order to obtain insight into the cellular functions of the BBSome, we attempted to map detailed interactions among BBSome subunits. However, the subunit interaction data obtained using the yeast two-hybrid system were unreliable (see supplementary material Fig. S1), and BBS proteins expressed in *Escherichia coli* were largely insoluble. By contrast, BBSome subunits expressed as fluorescent fusion proteins in HEK293T cells were soluble. Hence, we analyzed binary interactions between BBSome subunits expressed as fluorescent fusion proteins in HEK293T cells. During the course of these analyses, we sought to establish a novel and versatile assay to visualize protein–protein interactions based on immunoprecipitation, without requiring immunoblotting. Using this versatile assay system, which we named the visible immunoprecipitation (VIP) assay, we mapped the detailed interactions of the BBSome and exocyst subunits. The simple VIP assay established here will contribute to understanding of the architectures of various multisubunit complexes involved in a variety of cellular processes, and drive functional studies by

Graduate School of Pharmaceutical Sciences, Kyoto University, Kyoto 606-8501, Japan.
*These authors contributed equally to this work

‡Author for correspondence (kazunaka@pharm.kyoto-u.ac.jp)

Received 12 January 2015; Accepted 30 April 2015

Journal of Cell Science

Journal of Cell Science (2015) 128, 2351-2362 doi:10.1242/jcs.168740

validating protein networks predicted from unbiased global analyses of protein–protein interactions.

RESULTS

Unreliable BBSome subunit interaction data obtained using the yeast two-hybrid system

Our initial attempts to reveal interactions between BBSome subunits using GST pulldown assays were unsuccessful, because none of the examined BBSome subunits fused to GST were soluble in *E. coli*. Next, we attempted to determine BBSome subunit interactions using the yeast two-hybrid system, but failed to obtain reliable interaction data (supplementary material Fig. S1): (1) an interaction between BBS8 and BBS9, which have been reported to form a stoichiometric complex in a co-immunoprecipitation assay (Nachury et al., 2007), was detected when they were expressed as fusion proteins with the Gal4 DNA-binding domain and activation domain, respectively, but not when the two proteins were expressed in a reverse bait–prey configuration; (2) the interaction between BBS2 and BBS7, which have also been reported to form a stoichiometric complex (Nachury et al., 2007), was not detected in either of the bait–prey configurations; and (3) BBS5 elicited self-activation when expressed as a fusion with the DNA-binding domain.

Outline of a novel method for visualizing protein–protein interactions

An outline of a novel method to determine protein–protein interactions without performing immunoblotting is summarized in Fig. 1. Expression vectors for two proteins (protein X and protein Y) fused to EGFP and tagRFP (tRFP), respectively, were transfected into cultured cells (e.g. HEK293T cells). Expression of these fusion proteins can be confirmed in living cells by observing the transfectants under a fluorescence microscope (Fig. 2A). At this step and/or the following immunoprecipitation step with anti-GFP nanobody (see Fig. 2B), considerable variability in the expression levels of fluorescent fusion proteins can be reproducibly observed. In such cases, changing the promoter of the expression vector to a stronger one (e.g. the CAG promoter) often improves the protein expression level. However, in our experience, the expression level of one protein sometimes varies when co-expressed protein is different.

Lysates prepared from the transfected cells were then processed for immunoprecipitation. As an alternative to conventional anti-GFP antibodies, we exploited anti-GFP nanobody, which is a GFP-binding protein derived from a llama single-heavy chain antibody, and whose primary and three-dimensional structures are open (Kubala et al., 2010; Saerens et al., 2005); we expressed and purified anti-GFP nanobody fused to GST in *E. coli* (see Materials and Methods). Cell lysates containing EGFP and tRFP fusion proteins were pulled down with GST-tagged anti-GFP nanobody pre-bound to glutathione–Sepharose-4B beads. Instead of performing SDS–polyacrylamide gel electrophoresis and subsequent immunoblotting (Fig. 1C), we directly observed beads bearing immunoprecipitates under a fluorescence microscope (Fig. 1A; for example, see Fig. 2B) or a confocal laser-scanning microscope (for an example, see Fig. 4). If protein X interacts with protein Y, not only the EGFP signal but also the tRFP signal is detectable on the surface or perimeter of the beads. By

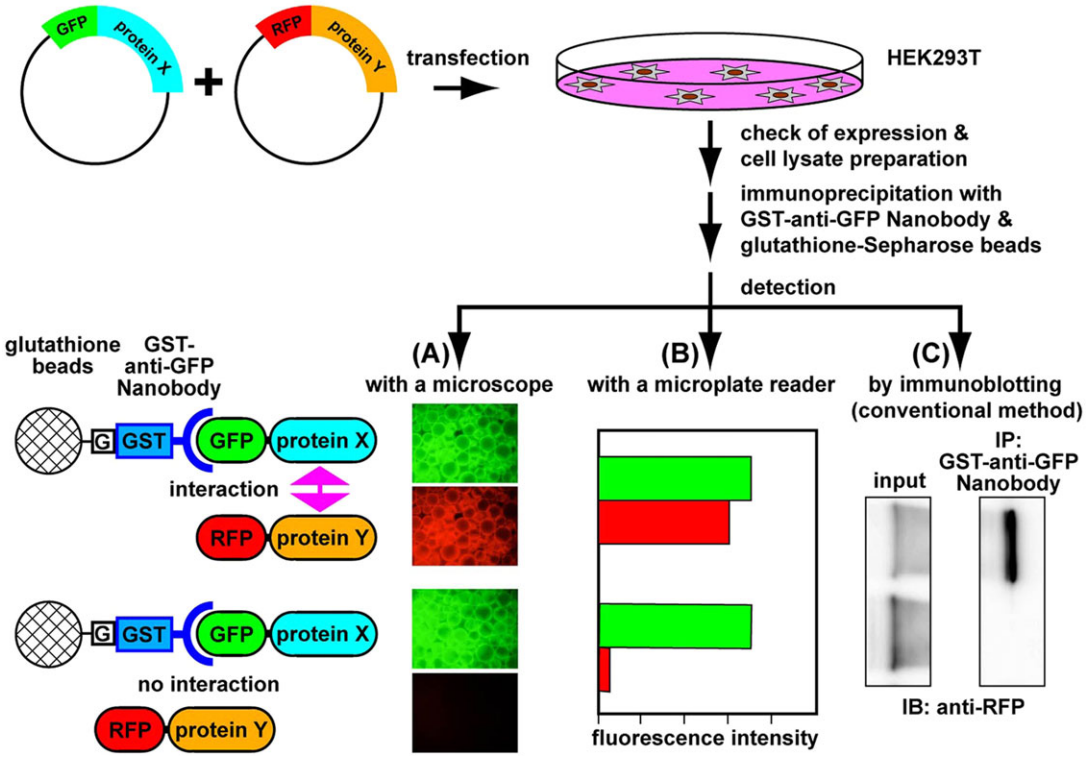

Fig. 1. Outline of the 'visible' immunoprecipitation assay. HEK293T cells were transfected with expression vectors for proteins X and Y, fused to GFP and RFP, respectively. After expression of the fluorescent fusion proteins was confirmed under a fluorescence microscope, cell lysates were prepared and processed for immunoprecipitation with GST-tagged anti-GFP nanobody pre-bound to glutathione–Sepharose-4B beads. (A) Beads bearing immunoprecipitates were directly observed with a fluorescent microscope. If protein X interacted with protein Y, both the green and red signals were detected on the surface or perimeter of the beads. If protein X did not interact with protein Y, only the green signal was detected. (B) Beads bearing immunoprecipitates were placed in a 96-well plate, and the fluorescence intensity in each well was measured using a fluorescence microplate reader. (C) Proteins bound to the precipitated beads were processed for conventional immunoblotting: SDS-PAGE, electroblotting onto a membrane and detection with an anti-RFP antibody.

Journal of Cell Science

Journal of Cell Science (2015) 128, 2351-2362 doi:10.1242/jcs.168740

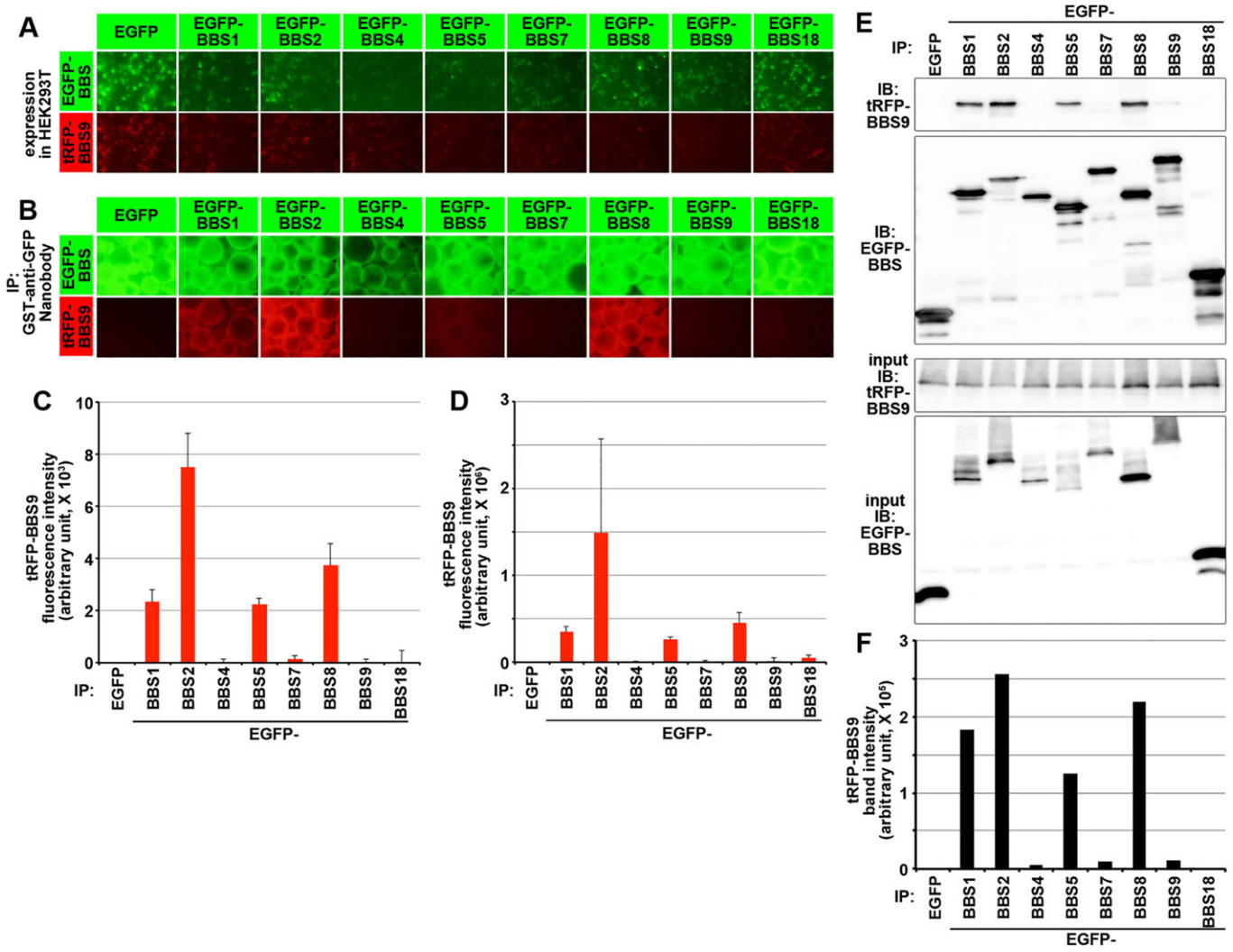

Fig. 2. Interactions of BBS9 with other BBSome subunits revealed by the VIP assay. HEK293T cells cultured in six-well plates were transfected with expression vectors for tRFP–BBS9 and either EGFP or each BBSome subunit fused to EGFP, as indicated. (A) At 24 h after transfection, expression of the green and red fluorescent fusion proteins were confirmed using a BZ-8000 all-in-one–type fluorescence microscope. Lysates prepared from the transfected cells were precipitated with GST-tagged anti-GFP nanobody pre-bound to glutathione–Sepharose-4B beads. (B) Beads bearing immunoprecipitates were observed, and the beads images were acquired, using a BZ-8000 microscope under fixed conditions (for green fluorescence, sensitivity ISO 400, exposure 1/30 s; and for red fluorescence, sensitivity ISO 800, exposure 1/10 s). (C) Red fluorescence intensities in the acquired images were measured using Image J and is expressed as bar graphs. From each value, the value of fluorescence intensity obtained from cells expressing EGFP and tRFP–BBS9 was subtracted as background. (D) Fluorescence intensities on the precipitate beads were measured directly, using a microplate reader. The values were expressed as bar graphs as in C. In C and D, the values are means±s.d. of three independent experiments. (E) Proteins bound to the precipitated beads (upper two panels) or input proteins (10%; lower two panels) were processed for immunoblotting with antibodies to tRFP (top and third panels) or GFP (second and bottom panels). (F) The band intensities in the top panel in E were quantified using ImageJ and expressed as bar graphs.

contrast, if protein X does not interact with protein Y, only the EGFP signal is detected. The relative intensities of the interactions can be roughly estimated by quantifying the fluorescence signals in the acquired bead images (Fig. 2C) or by subjecting the beads to measurement of fluorescence intensities with a microplate reader (Fig. 1B; Fig. 2D).

Application of the VIP assay to determine binary interactions of BBSome subunits

We first verified the effectiveness and reproducibility of the VIP assay by examining interactions of BBS9 with other BBSome subunits. An earlier study characterizing the BBSome has suggested that BBS9 is the central organizing subunit of the BBSome (Nachury et al., 2007). Expression vectors for BBS9 N-terminally tagged with tRFP and each of the eight BBSome subunits N-terminally tagged with EGFP were co-transfected into HEK293T cells. After protein expression was confirmed in living cells by fluorescence microscopy (Fig. 2A), lysates prepared from the transfected cells were subjected to immunoprecipitation using GST-tagged anti-GFP nanobody pre-bound to glutathione–Sepharose beads. Images of beads bearing immunoprecipitates were then acquired using the same microscope and exposure times. As shown in Fig. 2B, the tRFP–BBS9 signal on the precipitated beads was detectable at varying intensities when tRFP–BBS9 was co-expressed with EGFP-tagged BBS1, BBS2, BBS5 and BBS8. The rank order of the intensities of the BBS9 interactions, roughly determined by quantitation of red signal intensities of the acquired images, was BBS2>BBS8>BBS1≥BBS5 (Fig. 2C). When beads bearing immunoprecipitates were subjected to direct measurement of the fluorescence intensities with a microplate reader, the same rank order was obtained (Fig. 2D).

Journal of Cell Science (2015) 128, 2351-2362 doi:10.1242/jcs.168740

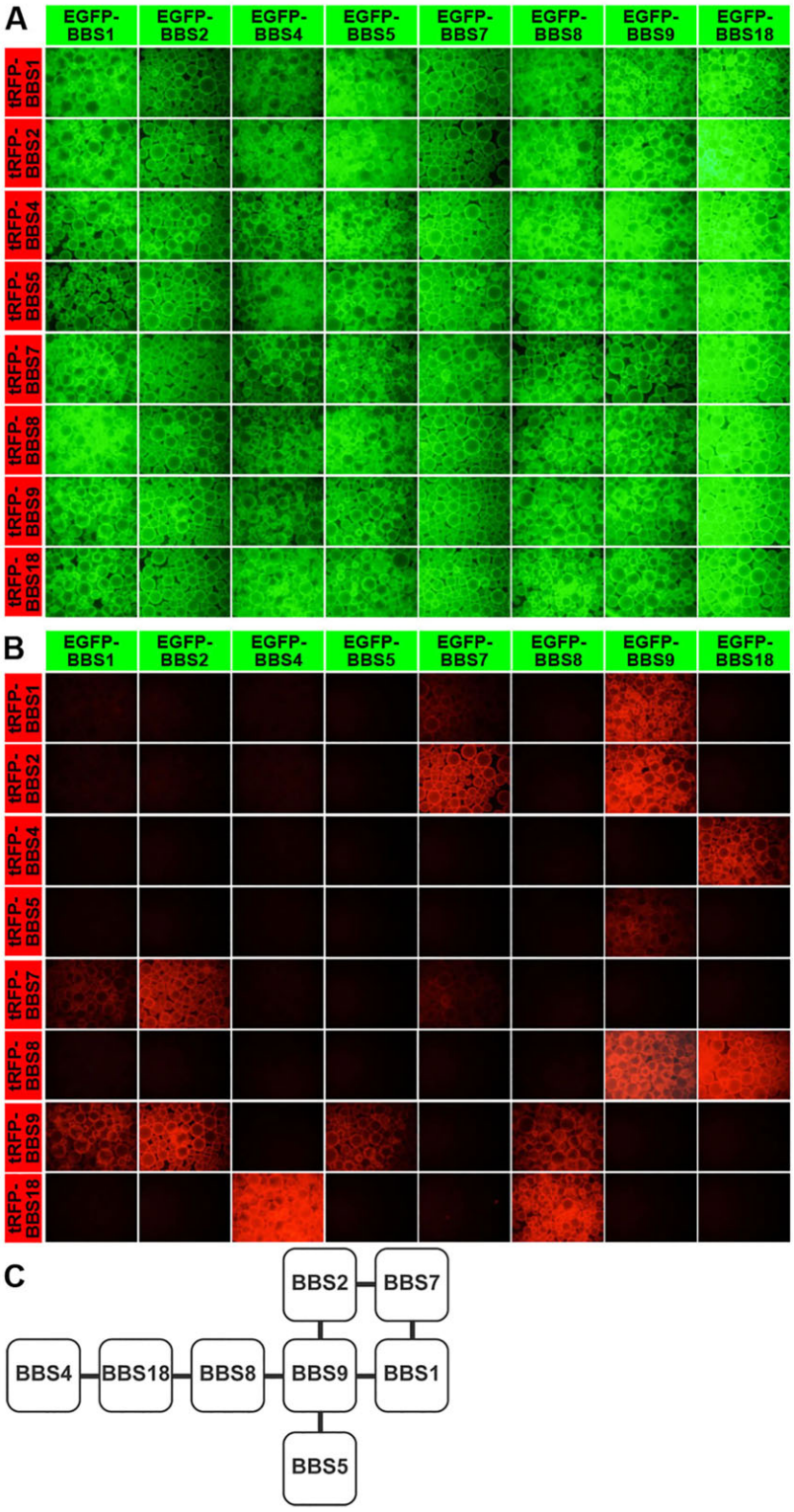

Fig. 3. All-by-all VIP assays of BBSome subunits. HEK293T cells cultured in six-well plates were transfected with expression vectors for tRFP- and EGFP-tagged BBSome subunits, as indicated. After expression of the green and red fluorescent fusion proteins was confirmed, lysates were prepared from the transfected cells and precipitated with GST-tagged anti-GFP nanobody pre-bound to glutathione–Sepharose beads. The green (A) and red (B) fluorescence signals on the precipitated beads were observed, and the bead images were acquired, using a BZ-8000 microscope. The experiments were repeated twice, and essentially the same results were obtained. (C) The BBSome subunit interaction map predicted from the data shown in B.

We then confirmed the tRFP–BBS9 interactions with other BBSome subunits tagged with EGFP by co-immunoprecipitation followed by conventional immunoblotting. As shown in Fig. 2E, the tRFP–BBS9 band was detected when lysates of cells co-expressing EGFP–BBS1, –BBS2, –BBS5 or –BBS8 were subjected to immunoprecipitation with GST-tagged anti-GFP nanobody (top panel). Although relative expression levels (Fig. 2E, bottom panel) and amounts in the precipitates (second panel) of the EGFP–BBS proteins varied from protein to protein, the rank order of the relative band intensities (Fig. 2F) was roughly parallel with that determined by the VIP assay (Fig. 2C,D). Taken together, these results support the idea that the VIP assay is a convenient, reproducible, and qualitative or semi-quantitative alternative to conventional co-immunoprecipitation followed by immunoblotting. Because the most important point is that this assay is handy and convenient, we did not further investigate

Journal of Cell Science

Journal of Cell Science (2015) 128, 2351-2362 doi:10.1242/jcs.168740

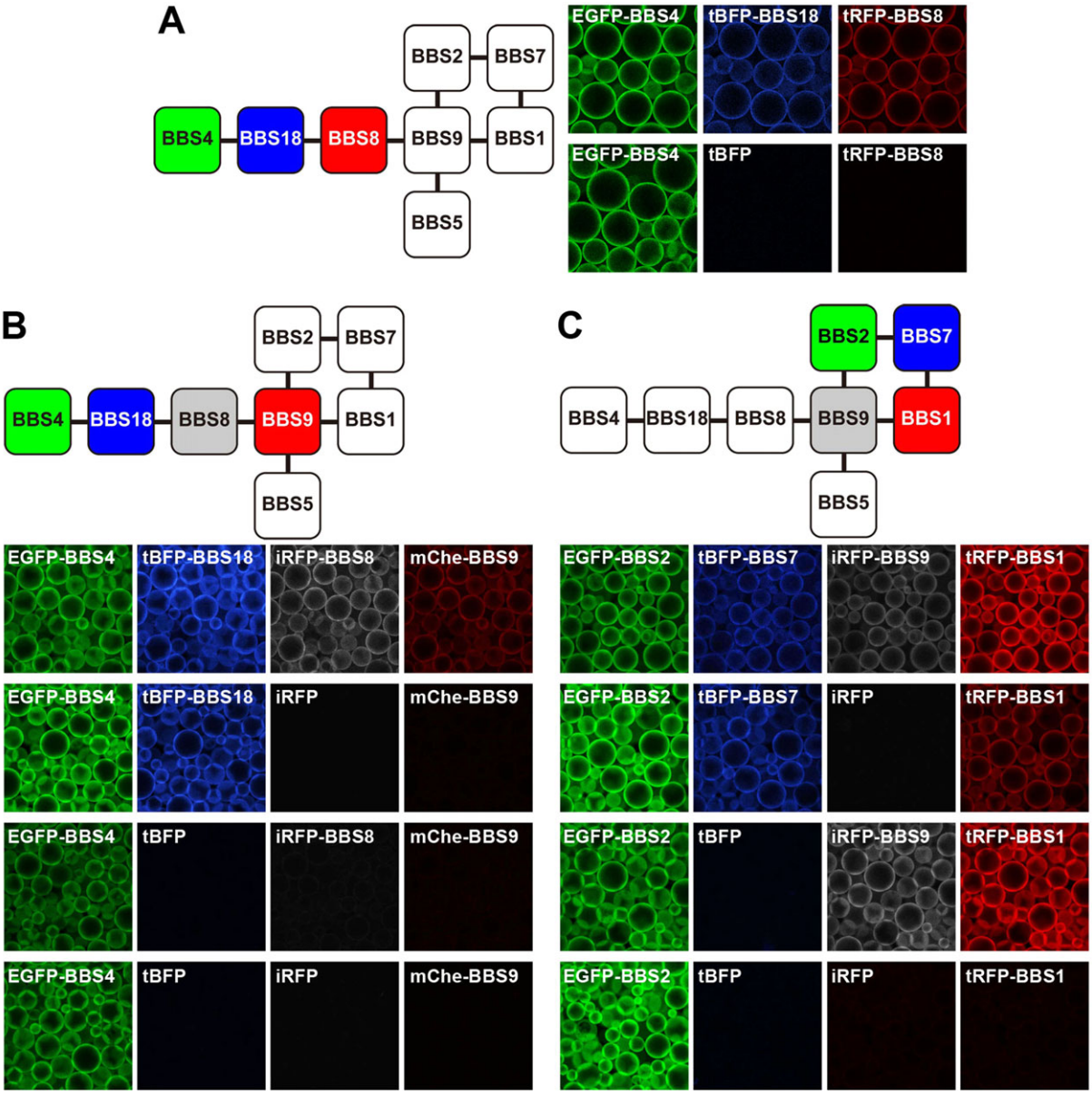

Fig. 4. Visible three- and four-hybrid assays of BBSome subunits. (A) HEK293T cells grown on 6-cm dishes were transfected with expression vectors for EGFP–BBS4, tRFP–BBS8 and either tBFP–BBS18 (upper panels) or tBFP (lower panels). After expression of the green and red fluorescent fusion proteins was confirmed, lysates were prepared from the transfected cells and precipitated with GST-tagged anti-GFP nanobody pre-bound to glutathione–Sepharose beads. The green (left), blue (middle) and red (right) fluorescence signals on the precipitated beads were observed, and the bead images were acquired using an A1R-MP confocal laser-scanning microscope. (B) HEK293T cells grown in 6-cm dishes were transfected with expression vectors for EGFP–BBS4, mCherry–BBS9, either tBFP–BBS18 or tBFP, and either iRFP–BBS8 or iRFP, as indicated, and then processed as described in A. The signals for EGFP (left), tBFP (second column), iRFP (third column), and mCherry (right) on the precipitated beads were acquired using a confocal microscope. (C) HEK293T cells grown in 6-cm dishes were transfected with expression vectors for EGFP–BBS2, tRFP–BBS1, either tBFP–BBS7 or tBFP, and either iRFP–BBS9 or iRFP, as indicated, and then processed as described in A. The signals for EGFP (left), tBFP (second column), iRFP (third column) and tRFP (right) on the precipitated beads were acquired using a confocal microscope. These experiments were repeated twice, and essentially the same results were obtained.

whether there is a linear relationship between the strength of the interactions (the affinity of the proteins) and the fluorescence intensity of the precipitated beads. More quantitative methods, such as surface plasmon resonance and/or isothermal titration calorimetry, will be needed to measure precise affinity, stoichiometry, and the kinetics of the interactions between bait and prey proteins.

To obtain insight into the detailed architecture of the BBSome, we examined the 64 possible combinations of BBSome subunits using the VIP assay (Fig. 3A,B). In striking contrast to the results obtained using the yeast two-hybrid system (supplementary material Fig. S1), all of the detectable binary interactions between EGFP- and tRFP-tagged BBSome subunits were also detected using reverse combinations of the fluorescent protein tags (Fig. 3B). Except for a weak interaction between EGFP–BBS7 and tRFP–BBS7, none of the BBSome subunits exhibited a homophilic interaction. Because the expression levels of fluorescent fusion proteins sometimes vary depending on co-expressed proteins, we routinely qualify binary interactions as ‘positive’ when red fluorescent signals are visible on the perimeter of precipitated beads in reciprocal combinations of bait and prey fusion proteins under fixed conditions (see Materials and Methods, and the legend

Journal of Cell Science (2015) 128, 2351-2362 doi:10.1242/jcs.168740

for Fig. 2B). Therefore, interactions that are not qualified as positive do not always mean that the two proteins do not interact with each other.

A model of the BBSome architecture predicted from the interaction data is schematically shown in Fig. 3C. The following features are evident: (1) BBS9 is the hub subunit of the BBSome, as suggested by the initial BBSome study (Nachury et al., 2007); (2) the core subcomplex consists of BBS1, BBS2, BBS7, and BBS9, all of which share some structural features with subunits of the clathrin adaptor complexes and the COPI coat complex (Jin et al., 2010); (3) BBS18 and BBS8 serve as connectors between BBS4 and BBS9; and (4) BBS5, which has a phosphoinositide-binding pleckstrin homology (PH) domain (Nachury et al., 2007), is located at the periphery of the core subcomplex.

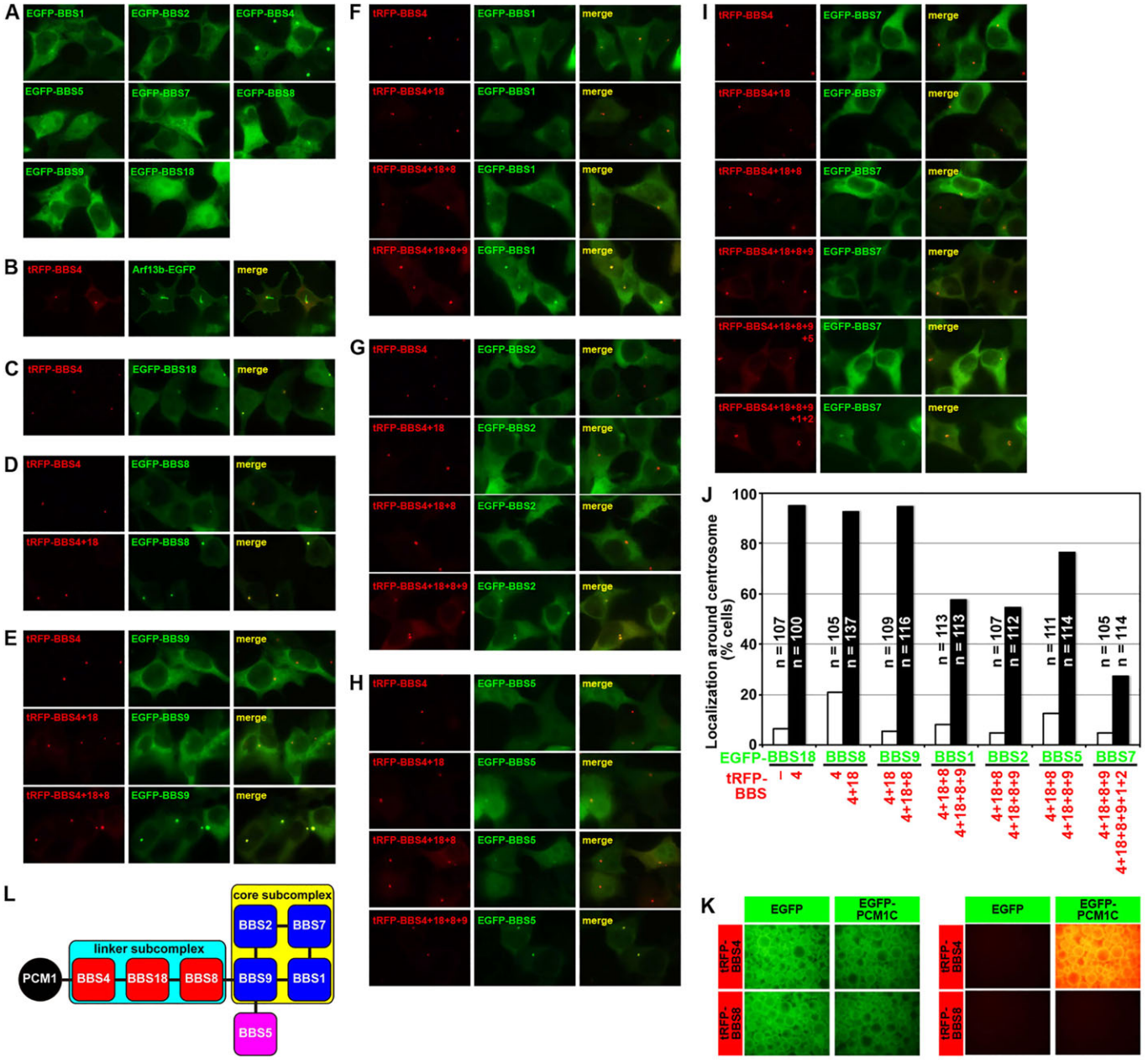

Fig. 5. Construction of the BBSome on the basis of centrosome-localized BBS4. (A) HEK293T cells transfected with an expression vector for each BBSome subunit fused to EGFP were observed under a fluorescence microscope. (B) HEK293T cells transfected with expression vectors for tRFP–BBS4 and Arl13b–EGFP. (C) HEK293T cells transfected with expression vectors for tRFP–BBS4 and EGFP–BBS18. (D) HEK293T cells transfected with expression vectors for tRFP–BBS4 and EGFP–BBS8 (upper panels), or those two proteins together with tRFP–BBS18 (lower panels). (E) HEK293T cells transfected with expression vectors for EGFP–BBS9 and the indicated BBSome subunit(s) fused to tRFP. (F) HEK293T cells transfected with expression vectors for EGFP–BBS1 and the indicated BBSome subunit(s) fused to tRFP. (G) HEK293T cells transfected with expression vectors for EGFP–BBS2 and the indicated BBSome subunit(s) fused to tRFP. (H) HEK293T cells transfected with expression vectors for EGFP–BBS5 and the indicated BBSome subunit(s) fused to tRFP. (I) HEK293T cells transfected with expression vectors for the indicated EGFP–BBS7 and BBSome subunit(s) fused to tRFP. (J) For the experiments shown in panels B–I, cells with and without centrosomal signals for the EGFP-tagged BBS proteins were counted, and the percentage of positive cells is expressed as a bar graph. (K) HEK293T cells cultured in six-well plates were transfected with expression vectors for either EGFP or EGFP–PCM1C and either tRFP–BBS4 or –BBS8, and processed as described in the legend for Fig. 3A,B. (L) Architecture of the BBSome predicted from the data shown in Figs 2–5.

Journal of Cell Science

Journal of Cell Science (2015) 128, 2351-2362 doi:10.1242/jcs.168740

Application of VIP assay to determine ternary and quaternary interactions of BBSome subunits

One notable feature of the BBSome model delineated above is that BBS18 is a component of the BBSome that serves as a linker between BBS4 and BBS8, both of which are almost entirely composed of tetratricopeptide repeats. BBS18, which was originally referred to as BBIP10 (for BBSome-interacting protein of 10 kDa), was missed in the initial BBSome isolation (Nachury et al., 2007), but was identified as a component of the BBSome in a subsequent study (Loktev et al., 2008) and has been recently found to be mutated in BBS patients (Scheidecker et al., 2014). However, Loktev et al. also reported that BBS18 associates with the BBSome inside the cilium, but not at centriolar satellites (Loktev et al., 2008).

To confirm that BBS18 is an integral component of the BBSome, we then applied the VIP assay to predicted ternary interactions of BBS4, BBS18 and BBS8. To this end, we co-expressed these proteins as EGFP, tagBFP (tBFP) and tRFP fusions in HEK293T cells, and subjected the cell lysates to precipitation with GST–anti-GFP nanobody. As shown in Fig. 4A, tRFP–BBS8 was co-precipitated with EGFP–BBS4 when tBFP–BBS18 was co-expressed (upper panels). In striking contrast, tRFP–BBS8 was not precipitated at all when co-expressed with tBFP in place of tBFP–BBS18 (lower panels). Thus, our results unequivocally show that BBS18 is essential for connecting BBS4 and BBS8.

We then applied the VIP assay to the quaternary interactions of BBSome subunits in order to delineate the BBSome architecture. To this end, each of four BBS subunits was fused to EGFP, tBFP, infrared-RFP (iRFP), or tRFP or mCherry. We first examined the predicted linear interactions of BBS4, BBS18, BBS8 and BBS9. As shown in Fig. 4B, mCherry–BBS9 was co-precipitated with EGFP–BBS4 in the presence of co-expressed tBFP–BBS18 and iRFP–BBS8 (top panels). In marked contrast, mCherry–BBS9 was not co-precipitated at all in the absence of either tBFP–BBS18 (second row) or iRFP–BBS8 (third row), or both (bottom panels). Thus, these results confirm the linear interactions, BBS4–BBS18–BBS8–BBS9, predicted from the binary interaction data.

We next examined the predicted circular interactions of BBS9, BBS2, BBS7 and BBS1. As shown in Fig. 4C, tRFP–BBS1 co-precipitated with EGFP–BBS2 in the presence of co-expressed tBFP–BBS7 and iRFP–BBS9 (top panels). Unlike the case of the linear interactions shown in Fig. 4B, tRFP–BBS1 was co-precipitated with EGFP–BBS2 in the absence of either iRFP–BBS9 (second row) or tBFP–BBS7 (third row). However, tRFP–BBS1 was not co-precipitated in the absence of both iRFP–BBS9 and tBFP–BBS7 (bottom panels). These results confirm the predicted circular interactions: BBS1 can interact indirectly with BBS2 in two ways, namely, through BBS7 and BBS9.

Thus, the VIP assay is a powerful tool, not only for revealing binary protein–protein interactions but also for determining the order and/or hierarchy of those interactions. The assays using three or four distinct fluorescent fusion proteins can thereby be referred to as visible ‘three-hybrid’ or ‘four-hybrid’ assays, respectively.

Construction of the BBSome on the basis of centrosome-localized BBS4

The VIP assay data presented so far successfully delineated the architecture of the BBSome. We next investigated whether the hierarchy of the interactions thus predicted holds true under intracellular conditions. For this purpose, we exploited the fact that exogenously expressed BBS4 is localized at centriolar satellites around the centrosome (Kim et al., 2004; Zhang et al., 2012). When exogenously expressed in HEK293T cells, EGFP–BBS4 was localized around the centrosome, whereas none of other BBSome subunits expressed as EGFP fusions exhibited a typical pericentrosomal localization (Fig. 5A). tRFP–BBS4 was also observed around the basal body (Fig. 5B).

When co-expressed with tRFP–BBS4, a significant fraction of EGFP–BBS18 was localized around the centrosome (Fig. 5C,J); likewise, a significant fraction of EGFP–BBS8 became localized around the centrosome when co-expressed with tRFP–BBS4 and –BBS18, but not when co-expressed with tRFP–BBS4 alone (Fig. 5D,J). A significant fraction of EGFP–BBS9 was localized around the centrosome when co-expressed with tRFP–BBS4, –BBS18, and –BBS8, but not when co-expressed with tRFP–BBS4 and –BBS18 (Fig. 5E,J). Less efficiently, however, fractions of EGFP–BBS1, –BBS2 and –BBS5 (Fig. 5F–H, respectively, and Fig. 5J) were localized around the centrosome when co-expressed with tRFP–BBS4, –BBS18, –BBS8 and –BBS9, but not when co-expressed with tRFP–BBS4, –BBS18 and –BBS8. Finally, although much less efficiently, EGFP–BBS7 was detectable around the centrosome when co-expressed with tRFP–BBS4, –BBS18, –BBS8, –BBS9, –BBS1 and –BBS2, but not when tRFP–BBS1 and –BBS2 were omitted (Fig. 5I,J).

Previous studies have shown that BBS4 interacts with the C-terminal region of pericentriolar material 1 (PCM1) and localizes at centriolar satellites around the centrosome and basal body (Kim et al., 2004; Zhang et al., 2012). By contrast, another study has reported that the same C-terminal region of PCM1 interacts with BBS8 (Ansley et al., 2003). Therefore, we examined whether the PCM1 C-terminal region interacts with BBS4 or BBS8, or both. As shown in Fig. 5K, the VIP assay showed that EGFP–PCM1C can interact with BBS4, but not with BBS8. Taken together with the data shown in Fig. 5A–I, we conclude that the BBSome can localize around the centrosome on the basis of centrosome-localizing BBS4 (Fig. 5L), although our data cannot discriminate between two possibilities: (1) the BBSome is constructed around the centrosome and/or basal body, or (2) the pre-assembled BBSome is recruited en bloc to the centrosome and/or basal body. We favor the former possibility, because components of the BBS–chaperonin complex, which is required for BBSome assembly (Seo et al., 2010; Zhang et al., 2012), are localized around the basal body (Marion et al., 2009).

Application of the VIP assay to determine binary interactions of exocyst subunits

We next applied the VIP assay to reveal the architecture of another multisubunit complex, the exocyst. The exocyst complex, which is composed of eight subunits, is involved in tethering of exocytic vesicles to the plasma membrane for secretion (Heider and Munson, 2012; Liu and Guo, 2012). Although the interactions among exocyst subunits have been studied using the yeast two-hybrid system and biochemical binding assays (Matern et al., 2001; Munson and Novick, 2006; Vega and Hsu, 2001), the current subunit interaction map remains highly speculative (Liu and Guo, 2012; Munson and Novick, 2006).

We first examined 64 possible combinations of exocyst subunits fused to EGFP and either tRFP or mCherry. As shown in Fig. 6, the VIP assay revealed various binary interactions; some, such as Sec8–Sec10 and Sec10–Sec15, have been suggested in previous studies (Matern et al., 2001; Vega and Hsu, 2001), whereas others, such as Sec3–Sec6, have not been previously reported. It is also notable that, unlike the case of the BBSome, some exocyst subunits (Sec3, Sec8, Sec10 and Exo70) exhibited robust homophilic interactions. These results are compatible with a previous crystallographic study showing that the N-terminal region of yeast Sec3 dimerizes through domain swapping (Baek et al., 2010), and

Journal of Cell Science (2015) 128, 2351-2362 doi:10.1242/jcs.168740

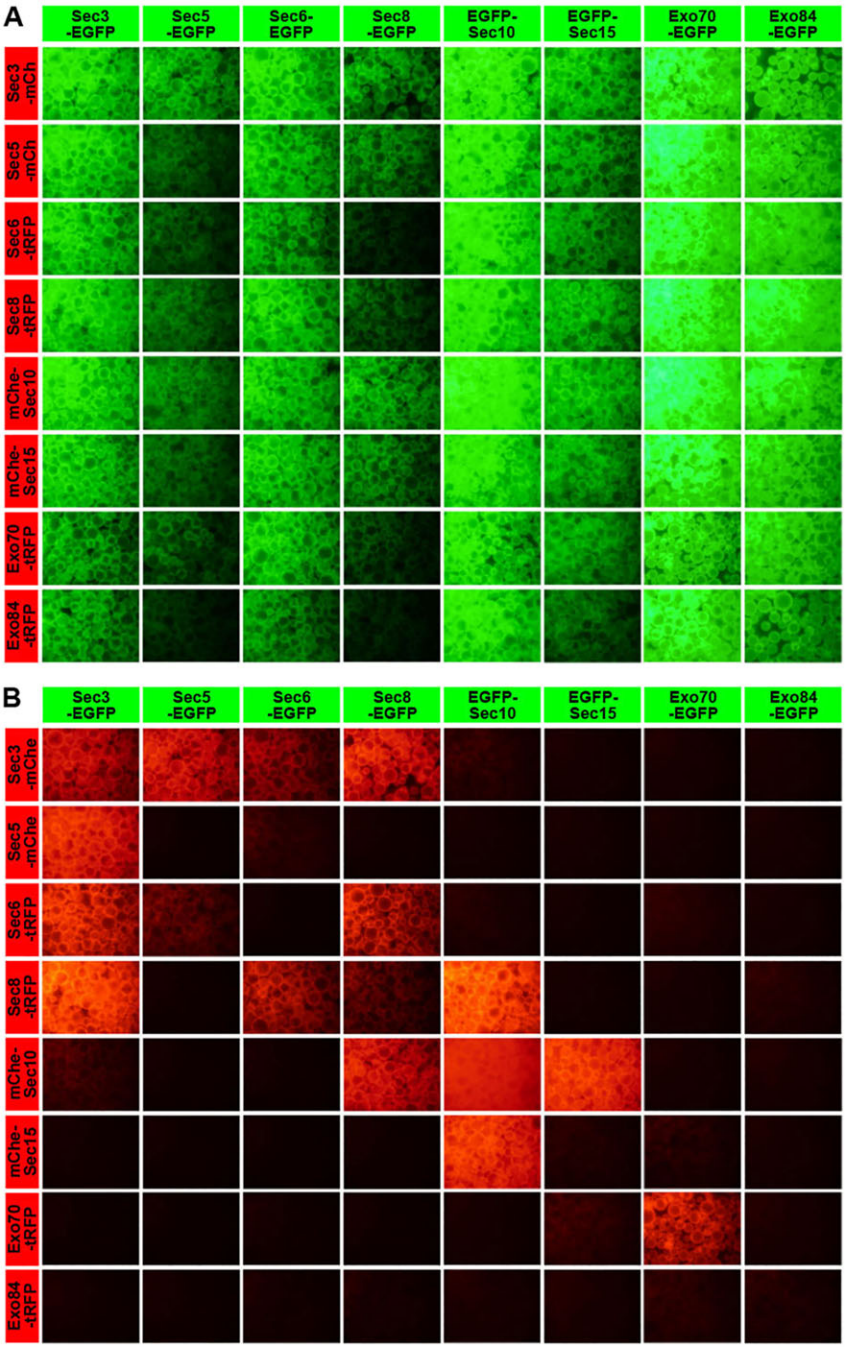

Fig. 6. All-by-all VIP assays of exocyst subunits. HEK293T cells cultured in six-well plates were transfected with expression vectors for exocyst subunits fused to EGFP and either mCherry or tRFP, as indicated, and processed as described in the legend for Fig. 3A,B. The experiments were repeated twice, and essentially the same results were obtained.

with identification of Sec10–Sec10 interaction by a recent high-quality interactome (Rolland et al., 2014).

In addition to strong interactions detected unequivocally by the VIP assay, there were also weakly detected interactions, such as those of Sec3–Sec10 and Sec5–Sec6. In the context of these weak interactions, the perimeters of precipitated beads were faintly decorated in red (Fig. 6B). We cannot exclude the possibility that these weak interactions were indirect and mediated by endogenous exocyst subunits present in non-transfected cells, given that the Sec3–Sec8 and Sec8–Sec10 interactions, as well as the Sec5–Sec3 and Sec3–Sec6 interactions, appeared to be very strong. We did not further pursue this issue in this study. By contrast, some binary interactions, such as Sec5–Sec10 and Sec5–Exo70 detected in a previous study using *in vitro* translated yeast exocyst subunits (Guo et al., 1999) were not detected by the VIP assay. Although we do not know the exact reason for the discrepancy, one possible explanation is that yeast and mammalian exocyst complexes may differ in the details of their architecture, since overall amino acid identities of corresponding yeast and human subunits are very limited; for example, 20.2% for Sec5 (see supplementary material Table S1).

One versus multi-subunit interactions revealed by subtraction analysis

One important point to be noted in the binary subunit interaction analysis is that Exo70 or Exo84 did not exhibit any obvious interaction with other exocyst subunits, although Exo70 did undergo a homophilic interaction (Fig. 6B). This was somewhat unexpected, given that the exocyst complex contains both the Exo70 and Exo84 subunits (Hsu et al., 1998; Terbush et al., 2001). However, when Exo70–EGFP was co-expressed with all other

Journal of Cell Science (2015) 128, 2351-2362 doi:10.1242/jcs.168740

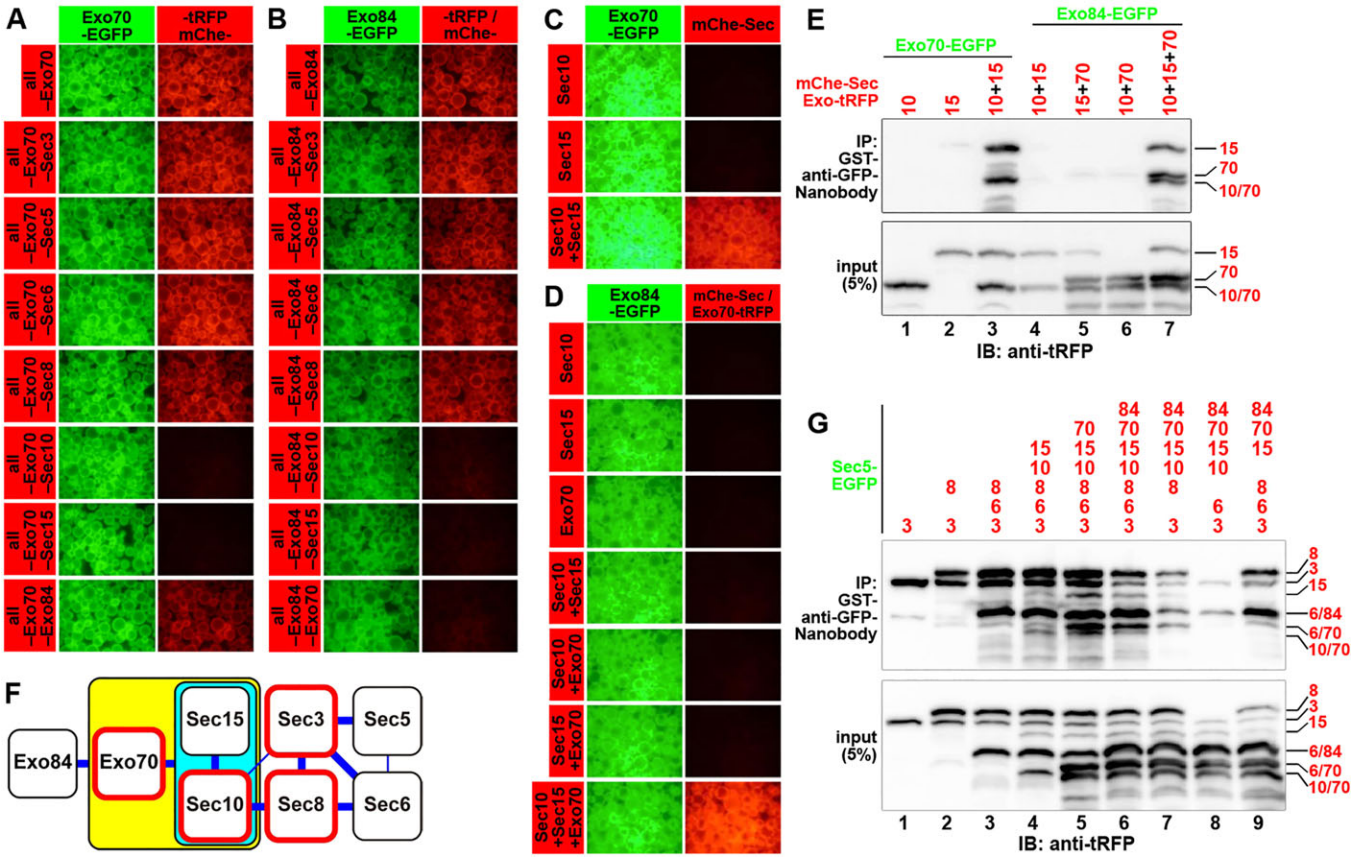

Fig. 7. One-to-many subunit interactions of exocyst subunits revealed by VIP assay. (A,B) HEK293T cells cultured in six-well clustered plates were transfected with expression vectors for either Exo70–EGFP (A) or Exo84–EGFP (B) and all but one (as indicated) of the other exocyst subunits fused to a red fluorescent protein (mCherry or tRFP as shown in Fig. 6), and then processed as described in the legend for Fig. 3A,B. (C–E) HEK293T cells cultured in six-well plates were transfected with expression vectors for either Exo70–EGFP (C,E, lanes 1–3) or Exo84–EGFP (D,E, lanes 4–7) and other exocyst subunit(s) (as indicated) fused to red fluorescent protein (mCherry or tRFP). At 24 h after transfection, lysates were prepared from the cells and precipitated with GST-tagged anti-GFP nanobody pre-bound to glutathione–Sepharose beads. (C,D) The green (left panels) and red (right panels) fluorescence signals on the precipitated beads were acquired using a BZ-8000 microscope. (E) Proteins bound to the precipitated beads (upper panel) or input proteins (5%; lower panel) were processed for immunoblotting with anti-tRFP antibody. Note that, for an unknown reason, Exo70–tRFP gave rise to two closely apposed bands, and the lower band was superimposed on the mCherry–Sec10 band. (F) The exocyst subunit interaction map predicted from the data shown in Fig. 6 and Fig. 7A–E. Exo70 can interact with the Sec10–Sec15 complex (shown in a light-blue box), and Exo84 with the Sec10–Sec15–Exo70 complex (shown in a yellow box). Sec3, Sec8, Sec10 and Exo70 exhibit homophilic interactions (surrounded by red lines), in addition to their heterophilic interactions with other subunits. The thickness of the blue line and red frame indicate the strengths of interactions and homophilic interactions, respectively. (G) HEK293T cells cultured in six-well plates were transfected with expression vectors for Sec5–EGFP and other exocyst subunit(s) (as indicated) fused to a red fluorescent protein (mCherry or tRFP), and then processed as described in E. In A–E and G, the experiments were repeated at least twice, and essentially the same results were obtained.

exocyst subunits fused to tRFP or mCherry in HEK293T cells, and subjected to immunoprecipitation with GST-tagged anti-GFP nanobody pre-bound to glutathione–Sepharose beads, distinct red fluorescent signals were observed on the precipitated beads (Fig. 7A, top panels). This result proves that Exo70 is indeed included in the exocyst complex. A similar experiment showed that Exo84 is also included in the exocyst complex (Fig. 7B, top panels).

To obtain insight into the interaction modes of Exo70 and Exo84 in the exocyst complex, we then performed the VIP assay when omitting one of the other subunits. As shown in Fig. 7A, red fluorescent signals were not observed on beads precipitated with Exo70–EGFP when either Sec10 (third row from the bottom) or Sec15 (second row from the bottom) was omitted. Similarly, red fluorescent signals on beads precipitated with Exo84–EGFP were extremely low when Sec10, Sec15 or Exo70 was omitted (Fig. 7B). These results raise the possibility that Exo70 interacts with a complex of Sec10 and Sec15, and that Exo84 interacts with a complex composed of Sec10, Sec15 and Exo70.

To determine whether Exo70 can interact with a complex of Sec10 and Sec15, we co-expressed Exo70–EGFP with mCherry-fused Sec10, mCherry-fused Sec15 or both proteins in HEK293T cells, and then subjected these cells to the VIP assay. As expected from the binary interaction assay (Fig. 6) and the subtraction analysis (Fig. 7A), Exo70–EGFP co-precipitated mCherry-fused proteins only when both mCherry–Sec10 and –Sec15 were co-expressed (Fig. 7C). Similar experiments were performed for Exo84. As shown in Fig. 7D, Exo84–EGFP co-precipitated red fluorescent fusion proteins when mCherry–Sec10, mCherry–Sec15 and Exo70–tRFP were simultaneously co-expressed, but did not co-precipitate when any one of the three red fluorescent exocyst subunits was omitted.

We then confirmed the VIP data by co-immunoprecipitation, followed by conventional immunoblotting. As shown in Fig. 7E, neither mCherry–Sec10 (lane 1) nor mCherry–Sec15 (lane 2) was co-immunoprecipitated by GST-tagged anti-GFP nanobody when co-expressed alone with Exo70–EGFP. In striking contrast, bands for both mCherry–Sec10 and –Sec15 were detected in the immunoprecipitate when both fusion proteins were co-expressed

Journal of Cell Science (2015) 128, 2351-2362 doi:10.1242/jcs.168740

(lane 3). Similarly, red fluorescent fusion proteins of Sec10, Sec15 and Exo70 were co-immunoprecipitated with Exo84–EGFP only when all the three fusion proteins were co-expressed with Exo84–EGFP (compare lane 7 with lanes 4–6; for an unknown reason, Exo70–tRFP gave rise to two closely apposed bands, and the lower band was superimposed on the band for mCherry–Sec10).

The map of interactions among the exocyst subunits predicted from the data presented here is shown in Fig. 7F. Among the eight subunits, Sec3, Sec5, Sec6, and Sec8 appear to form a tight quaternary subcomplex, and Sec10 and Sec15 form another subcomplex. These two subcomplexes appear to be connected through an interaction between Sec8 and Sec10, which has also been detected in previous yeast two-hybrid and biochemical interaction studies (Matern et al., 2001; Vega and Hsu, 2001). In the predicted interaction map, Exo70 and Exo84 are positioned peripherally to the Sec10–Sec15 subcomplex, as these subunits failed to show any binary interactions with other subunits, and can interact strongly with the Sec10–Sec15 subcomplex and the Sec10–Sec15–Exo70 subcomplex, respectively.

To corroborate the predicted exocyst model, we performed a set of co-immunoprecipitation experiments using lysates of cells co-expressing Sec5–EGFP and various combinations of other exocyst subunits fused to mCherry or tRFP. We chose Sec5 as a starting subunit for exocyst assembly, because it exhibits a strong interaction only with Sec3 (see Fig. 7F). As shown in Fig. 7G, by adding Sec3, Sec8 and Sec6 one after another, we could construct the core subcomplex composed of Sec3, Sec5, Sec6, and Sec8 (lanes 1–3). Sec10 and Sec15 were associated with the core subcomplex (compare lanes 3 and 4). Then, although this could not be conclusively determined due to overlap or close proximity of some bands, Exo70 and Exo84 were likely to be incorporated into the precipitated complex (lanes 4–6). When Sec6 was omitted from the full subunit set, Sec5–EGFP was still able to co-immunoprecipitate other subunits, although less effectively than in the presence of the full subunit set (compare lane 7 with lane 6). Exclusion of Sec8 from the full subunit set resulted in collapse of the complex, and only Sec3 and Sec6 co-immunoprecipitated with Sec5–EGFP (compare lane 8 with lane 6). By contrast, in the absence of Sec10, the core subcomplex was still constructed, although the co-immunoprecipitate did not include Sec15, Exo70 or Exo84 (lane 9). These results are, as a whole, consistent with the predicted model (Fig. 7F), in which the core subcomplex is linked to peripheral subunits through the Sec8–Sec10 interaction.

DISCUSSION

The ‘visible’ immunoprecipitation (VIP) assay we established on the basis of a combination of preexisting methods has several advantages over conventional qualitative protein–protein interaction assays, although it has some drawbacks compared with other qualitative assays as summarized in supplementary material Table S2, and more quantitative methods are required to measure the precise affinity, stoichiometry and kinetics of the interactions. First and most importantly, in contrast to pulldowns with GST fusion proteins and immunoprecipitation of epitope-tagged proteins, both of which are usually followed by immunoblotting to detect interacting proteins (see Fig. 1C), the VIP assay can detect interactions between GFP and RFP fusion proteins through direct observation of the immunoprecipitates (precipitated glutathione–Sepharose beads) under a fluorescence microscope (Fig. 1A). By omitting labor-intensive and time-consuming procedures, including electrophoresis, electroblotting, and incubation and detection with primary and secondary antibodies, we can detect protein–protein interactions the day after transfection of expression vectors into HEK293T cells, without the expenses associated with reproducibility. Measurements of fluorescence intensities emitted from the precipitates using a microplate reader can further speed up the detection process (Fig. 1B). In addition, confirmation of the expression levels of fluorescent fusion proteins in transfected cells is also time-saving relative to the use of epitope-tagged proteins: in the VIP assay, we can roughly determine expression levels of fluorescent fusion proteins by simply observing live transfected cells under a fluorescence microscope (see Fig. 2A), whereas confirmation of expression of epitope-tagged proteins usually requires cell lysis, electrophoresis and immunoblotting.

Second, the VIP assay can determine interactions between more than two proteins at one time. Using proteins fused to EGFP, tRFP, tBFP and iRFP, we could successfully determine not only the interactions themselves but also the hierarchy of the interactions between four BBSome subunits (see Fig. 4). Thus, by extending the concept of the visible ‘two-hybrid’ assay, we could establish visible ‘three-hybrid’ and ‘four-hybrid’ assays. In principle, the number of interactions to be determined at one time will increase along with the number of fluorescent proteins that have distinct excitation and emission profiles and can therefore be used simultaneously.

Third, the VIP assay can determine one-to-many protein interactions, which can only be detected using epitope-tagged proteins through tremendous effort. In particular, we could successfully determine one-to-many subunit interactions in the exocyst complex. Although neither Exo70– nor Exo84–EGFP exhibited any binary interactions with other exocyst subunits fused to mCherry or tRFP (Fig. 6), assays performed on lysates of cells co-expressing Exo70– or Exo84–EGFP and all other subunits fused to mCherry or tRFP showed that they both are indeed included in the complex (Fig. 7A,B). Subsequent subtraction analysis indicated subunits that are required for Exo70 or Exo84 to be included in the exocyst complex (Fig. 7A,B). Finally, one-to-many protein interaction assays unequivocally determined that Exo70 can interact with a complex of Sec10 and Sec15, and that Exo84 can interact with a complex composed of Sec10, Sec15 and Exo70 (Fig. 7C–E).

Fourth, because the VIP assay is a modified co-immunoprecipitation assay, it can detect protein–protein interactions that take place under intracellular conditions. This is in contrast to the conventional yeast two-hybrid assay, in which translocation of fusion proteins into the nucleus is prerequisite for activation of reporter gene expression. Because the VIP assay directly detects protein–protein interactions, it can considerably reduce the risk of detecting pseudo-positive interactions or missing genuine positive interactions, both of which are inherent to the yeast two-hybrid assay (compare Fig. 3 with supplementary material Fig. S1). The VIP assay is also superior to the GST-pulldown assay, which can detect protein–protein interactions *in vitro*. For example, we could detect the BBS8–BBS9 interaction using lysates of cells co-expressing EGFP–BBS8 and tRFP–BBS9, but not using a mixture of lysates from cells expressing EGFP–BBS8 and cells expressing tRFP–BBS9 (supplementary material Fig. S2). This difference might be attributable to the fact that the BBSome subunits require specific chaperones in order to be folded or assembled into the BBSome (Seo et al., 2010; Zhang et al., 2012).

Fifth, the VIP assay is based on common techniques readily available to molecular cell biologists. Because many fluorescent protein fusion vectors have already been constructed, one would not always need to construct new plasmids for the VIP assay. Furthermore, the bacterial expression vector for GST-tagged anti-GFP nanobody, which is used for immunoprecipitation of GFP fusion proteins, has been deposited in Addgene, making it available to all potential users. Although previous

Journal of Cell Science

Journal of Cell Science (2015) 128, 2351-2362 doi:10.1242/jcs.168740

studies have reported similar qualitative protein–protein interaction assays based on direct imaging of beads (Patel et al., 2007; Schulte et al., 2008; Zhou et al., 2013), bait proteins to detect fluorescence-tagged prey proteins were limited in these visual assays because bait proteins were first immobilized on the beads. By contrast, by using anti-GFP nanobody immobilized on the beads, a wide variety of GFP fusion proteins are available as bait in the VIP assay. Recently, more powerful single-molecule pulldown and co-immunoprecipitation analyses have been reported (Aggarwal and Ha, 2014; Lee et al., 2013). In these analyses, after immobilization of conventional anti-GFP or anti-mCherry antibody on the surface of quartz slide, cell lysates containing the bait protein tagged with YFP or mCherry and the prey protein tagged with mCherry or GFP were added, and proteins trapped by the immobilized antibody were visualized by total internal reflection fluorescence microscopy. Thus, unlike the VIP assay, these serve as single-molecule biochemical tools to enable absolute quantification of protein complexes. However, users of these single-molecule analyses are limited due to the use of total-internal reflection fluorescence microscopy, whereas the VIP assay does not require any special equipment, except for a conventional fluorescence microscope.

In addition to the aforementioned advantages, we have developed some techniques that save time and reduce the unit cost of the assay (for details, see Materials and Methods). For example, in place of normal anti-GFP antibody and protein A or G agarose beads, we used bacterially expressed GST-tagged anti-GFP nanobody pre-bound to glutathione–Sepharose beads. Nanobodies are camelid-derived single-domain immunoglobulins with a small size (~15 kDa) that are composed of heavy chain homodimers devoid of light chains. The virtually inexhaustible source of the anti-GFP antibody makes it possible to perform interaction assays on a large scale. Although previous studies have made use of anti-GFP nanobody to perform various interaction assays with low or medium throughput (Pichler et al., 2012; Rothbauer et al., 2008; Zolghadr et al., 2008), those studies were all limited to binary interactions. In this study, we made use of anti-GFP nanobody to co-immunoprecipitate up to eight proteins fused to up to four distinct fluorescent proteins, thereby elucidating the architectures of the BBSome and exocyst complexes. Thus, the simple, versatile VIP assay established here will not only pave the way to understanding the architectures and functions of various multisubunit complexes involved in a variety of cellular processes, but also drive functional studies by validating protein networks predicted from unbiased global protein–protein interaction analyses (e.g. see Rolland et al., 2014).

MATERIALS AND METHODS

Plasmids

The whole coding sequences of BBSome and exocyst subunits, listed in supplementary material Table S3, were amplified by PCR from human brain, kidney, or liver cDNA library and cloned into various types of fluorescent protein vectors: pEGFP-C1, pEGFP-N1 (Clontech), pcDNA3-EGFP-C, pTagRFP-T-C, pTagRFP-T-N (kind gifts from Hideki Shibata, Nagoya University, Japan) (Shibata et al., 2010), pCAG-mCherry-C (a kind gift from Roger Tsien, University of California - San Diego, CA) (Shaner et al., 2005), pTagBFP2-C (Evrogen), and pcDNA3-iRFP-C (a kind gift from Michiyuki Matsuda, Kyoto University, Japan). Plasmids used in this study are listed in supplementary material Table S4. For yeast two-hybrid assays, cDNAs of BBSome subunits were subcloned into pGBKT7 and pGADT7 (Clontech).

Antibodies

The following antibodies were obtained from the indicated vendors: monoclonal mouse anti-GFP (JL-8), BD Biosciences; polyclonal rabbit anti-tRFP antibody, Evrogen; and horseradish-peroxidase-conjugated secondary antibodies, Jackson ImmunoResearch Laboratories.

Preparation of GST-tagged anti-GFP nanobody beads

A DNA fragment encoding anti-GFP nanobody, synthesized based on the sequence previously (Kubala et al., 2010), was subcloned into pGEX-6P-1 (GE Healthcare). We have deposited the plasmid encoding GST-tagged anti-GFP nanobody to Addgene (ID number 61838). *E. coli* BL21(DE3) cells transformed with the GST-fused anti-GFP nanobody vector were treated with 0.1 mM IPTG for 4 h at 30°C to induce protein expression, lysed, and used to purify the recombinant protein with glutathione–Sepharose 4B beads (GE Healthcare). The yield of purified GST–anti-GFP nanobody was ~5 mg/l of bacterial culture. The protein concentration was adjusted to ~200 µg/ml for immunoprecipitation assays.

VIP assays

HEK293T cells, cultured in Dulbecco's modified Eagle's medium (DMEM) with high glucose (Nacalai Tesque) supplemented with 5% fetal bovine serum, were plated in six-well plates. Approximately 1.6×10^6 cells were transfected with EGFP (2 µg) and tRFP or mCherry (2 µg) fusion constructs using Polyethylenimine Max (20 µg) (Polysciences), and then cultured for 24 h. Before the assay, expression of fluorescent fusion proteins was confirmed under a fluorescence microscope. The cells were lysed in 250 µl of lysis buffer (20 mM HEPES-KOH pH 7.4, 150 mM NaCl, 0.1% Triton X-100 and 10% glycerol) containing protease inhibitor cocktail (Nacalai Tesque). After 15 min on ice, the cell lysates were centrifuged at 16,100 ***g*** for 15 min at 4°C in a microcentrifuge. The supernatants (200 µl) were incubated with 5 µl of GST-tagged anti-GFP nanobody pre-bound to glutathione–Sepharose 4B beads in 0.2 ml 8-Tube Strips (Greiner) for 1 h at 4°C. The tube strips were centrifuged at 2000 ***g*** for 30 s at room temperature. The precipitated beads were washed three times with 180 µl of lysis buffer, and then transferred into a 96-well plate for observation. Fluorescence on the beads was observed using an all-in-one type fluorescence microscope (Biozero BZ-8000, Keyence) using a 20×/0.75 NA objective lens under fixed conditions (for green fluorescence, sensitivity ISO 400, exposure 1/30 s; and for red fluorescence, sensitivity ISO 800, exposure 1/10 s). Image acquisition was performed under fixed conditions. The quantification of fluorescence intensity was performed using the ImageJ software (National Institutes of Health). Fluorescence was also measured with a microplate reader (EnVision, PerkinElmer) equipped with filter sets appropriate for detecting fluorescence. After fluorescence measurement, the materials bound to the beads were subjected to immunoblot analysis using anti-tRFP or anti-GFP antibody.

For expression of combinations of EGFP, tRFP or mCherry, tBFP and iRFP fusion constructs, approximately 3.2×10^6 HEK293T cells grown on 6-cm dishes were transfected with the expression vectors (12 µg) using Polyethylenimine Max (60 µg), and then cultured for 24 h. Immunoprecipitation was performed as described above. Fluorescence on the beads was measured with a confocal laser-scanning microscope (A1R-MP, Nikon) equipped with four lasers (405, 488, 561 and 638 nm wavelength) and using 20×/0.75 NA objective lens.

For expression of combinations of up to eight of EGFP and tRFP or mCherry fusion constructs, ~1.6×10^6 cells grown in 6-well plates were transfected with the expression vectors (8 µg) using Polyethylenimine Max (40 µg), and then cultured for 24 h. Immunoprecipitation was performed as described above.

Immunofluorescence microscopy

DNA transfection and immunofluorescence analysis of HEK293T cells were performed as described previously (Takahashi et al., 2012).

Immunoblotting

Proteins in cell lysates, prepared as described above, were separated by SDS-PAGE and electroblotted onto an Immobilon-P transfer membrane (Millipore). The membrane was blocked in 5% skimmed milk and incubated sequentially with primary and horseradish-peroxidase-conjugated secondary antibodies. Detection was carried out using a Chemi-Lumi One L kit (Nacalai Tesque).

Yeast two-hybrid assay

Yeast Y2H-Gold cells (Clontech) transformed with a pGBKT7-based bait vector were plated on synthetic defined medium lacking tryptophan (SD –W). Yeast Y187 cells transformed with pGADT7-based prey vector were plated on synthetic medium lacking leucine (SD –L). Colonies on

these plates were picked up, and bait and prey were mixed together in YPAD medium. The mated diploid cells were streaked on synthetic medium lacking tryptophan and leucine (SD –WL). The cells were replicated and grown on synthetic medium lacking tryptophan, leucine, histidine (SD –WLH), and adenine (SD –WLHA). Growth of cells on the selection plates was assessed after 2 or 3 days of incubation.

Acknowledgements
We would like to thank Michiyuki Matsuda, Hideki Shibata, and Roger Tsien for kindly providing materials, and Michiyuki Matsuda and Hye-Won Shin on critical comments on the manuscript. We also thank Yohei Hagiya, Minako Kobayashi, Takashi Matsumoto, Tomoki Naito, Minako Ohgi and Noriko Takahashi for technical assistance.

Competing interests
The authors declare no competing or financial interests.

Author contributions
Y.K. designed and performed experiments, and prepared the manuscript; S.N., D.H. and R.M. designed and performed experiments; and K.N. designed experiments and prepared the manuscript.

Funding
This work was supported in part by a Grant-in-Aid for Scientific Research on Innovative Areas 'Cilia and Centrosome' from the Ministry of Education, Culture, Sports, Science and Technology, Japan [grant number 25113514 to K.N.]; a grant from the Japan Society for Promotion of Science [grant number 22390013 to K.N.]; and a grant from the Uehara Memorial Foundation. This work was also indirectly supported by a Grant-in-Aid for Scientific Research on Innovative Areas 'Fluorescence Live imaging' from the Ministry of Education, Culture, Sports, Science and Technology of Japan.

Supplementary material
Supplementary material available online at
http://jcs.biologists.org/lookup/suppl/doi:10.1242/jcs.168740/-/DC1

References

Aggarwal, V. and Ha, T. (2014). Single-molecule pull-down (SiMPull) for new-age biochemistry. *Bioessays* **36**, 1109-1119.
Ansley, S. J., Badano, J. L., Blacque, O. E., Hill, J., Hoskins, B. E., Leitch, C. C., Kim, J. C., Ross, A. J., Eichers, E. R., Teslovich, T. M. et al. (2003). Basal body dysfunction is a likely cause of pleiotropic Bardet–Biedl syndrome. *Nature* **425**, 628-633.
Baek, K., Knödler, A., Lee, S. H., Zhang, X., Orlando, K., Zhang, J., Foskett, T. J., Guo, W. and Dominguez, R. (2010). Structure-function study of the N-terminal domain of exocyst subunit Sec3. *J. Biol. Chem.* **285**, 10424-10433.
Guo, W., Roth, D., Walch-Solimena, C. and Novick, P. (1999). The exocyst is an effector for Sec4p, targeting secretory vesicles to sites of exocytosis. *EMBO J.* **18**, 1071-1080.
Heider, M. R. and Munson, M. (2012). Exorcising the exocyst complex. *Traffic* **13**, 898-907.
Hong, W. and Lev, S. (2014). Tethering the assembly of SNARE complexes. *Trends Cell Biol.* **24**, 35-43.
Hsu, S.-C., Hazuka, C. D., Roth, R., Foletti, D. L., Heuser, J. and Scheller, R. H. (1998). Subunit composition, protein interactions, and structures of the mammalian brain sec6/8 complex and septin filaments. *Neuron* **20**, 1111-1122.
Jin, H. and Nachury, M. V. (2009). The BBSome. *Curr. Biol.* **19**, R472-R473.
Jin, H., White, S. R., Shida, T., Schulz, S., Aguilar, M., Gygi, S. P., Bazan, J. F. and Nachury, M. V. (2010). The conserved Bardet-Biedl syndrome proteins assemble a coat that traffics membrane proteins to cilia. *Cell* **141**, 1208-1219.
Kim, J. C., Badano, J. L., Sibold, S., Esmail, M. A., Hill, J., Hoskins, B. E., Leitch, C. C., Venner, K., Ansley, S. J., Ross, A. J. et al. (2004). The Bardet-Biedl protein BBS4 targets cargo to the pericentriolar region and is required for microtubule anchoring and cell cycle progression. *Nat. Genet.* **36**, 462-470.
Kubala, M. H., Kovtun, O., Alexandrov, K. and Collins, B. M. (2010). Structural and thermodynamic analysis of the GFP:GFP-nanobody complex. *Protein Sci.* **19**, 2389-2401.
Lee, H.-W., Kyong, T., Yoo, J., Kim, T., Chung, C., Ryu, J. Y., Lee, H., Park, K., Lee, S., Jones, W. D. et al. (2013). Real-time single-molecule co-immunoprecipitation analyses reveal cancer-specific Ras signalling dynamics. *Nat. Commun.* **4**, 1505.
Liu, J. and Guo, W. (2012). The exocyst complex in exocytosis and cell migration. *Protoplasma* **249**, 587-597.
Loktev, A. V., Zhang, Q., Beck, J. S., Searby, C. C., Scheetz, T. E., Bazan, J. F., Slusarski, D. C., Sheffield, V. C., Jackson, P. K. and Nachury, M. V. (2008). A BBSome subunit links ciliogenesis, microtubule stability, and acetylation. *Dev. Cell* **15**, 854-865.
Madhivanan, K. and Aguilar, R. C. (2014). Ciliopathies: the trafficking connection. *Traffic* **15**, 1031-1056.
Marion, V., Stoetzel, C., Schlicht, D., Messaddeq, N., Koch, M., Flori, E., Danse, J. M., Mandel, J.-L. and Dollfus, H. (2009). Transient ciliogenesis involving Bardet-Biedl syndrome proteins is a fundamental characteristic of adipogenic differentiation. *Proc. Natl. Acad. Sci. USA* **106**, 1820-1825.
Matern, H. T., Yeaman, C., Nelson, W. J. and Scheller, R. H. (2001). The Sec6/8 complex in mammalian cells: characterization of mammalian Sec3, subunit interactions. *Proc. Natl. Acad. Sci. USA* **98**, 9648-9653.
M'Hamdi, O., Ouertani, I. and Chaabouni-Bouhamed, H. (2014). Update on the genetics of Bardet-Biedl syndrome. *Mol. Syndromol.* **5**, 51-56.
Munson, M. and Novick, P. (2006). The exocyst defrocked, a framework of rods revealed. *Nat. Struct. Mol. Biol.* **13**, 577-581.
Nachury, M. V., Loktev, A. V., Zhang, Q., Westlake, C. J., Peränen, J., Merdes, A., Slusarski, D. C., Scheller, R. H., Bazan, J. F., Sheffield, V. C. et al. (2007). A core complex of BBS proteins cooperates with the GTPase Rab8 to promote ciliary membrane biogenesis. *Cell* **129**, 1201-1213.
Patel, S. S., Belmont, B. J., Sante, J. M. and Rexach, M. F. (2007). Natively unfolded nucleoporins gate protein diffusion across the nuclear pore complex. *Cell* **129**, 83-96.
Pichler, G., Jack, A., Wolf, P. and Hake, S. B. (2012). Versatile toolbox for high throughput biochemical and functional studies with fluorescent fusion proteins. *PLoS ONE* **7**, e36967.
Rolland, T., Taşan, M., Charloteaux, B., Pevzner, S. J., Zhong, Q., Sahni, N., Yi, S., Lemmens, I., Fontanillo, C., Mosca, R. et al. (2014). A proteome-scale map of the human interactome network. *Cell* **159**, 1212-1226.
Rothbauer, U., Zolghadr, K., Muyldermans, S., Schepers, A., Cardoso, M. C. and Leonhardt, H. (2008). A versatile Nanotrap for biochemical and functional studies with fluorescent fusion proteins. *Mol. Cell. Proteomics* **7**, 282-289.
Saerens, D., Pellis, M., Loris, R., Pardon, E., Dumoulin, M., Matagne, A., Wyns, L., Muyldermans, S. and Conrath, K. (2005). Identification of a universal VHH framework to graft non-canonical antigen-binding loops of camel single-domain antibodies. *J. Mol. Biol.* **352**, 597-607.
Scheidecker, S., Etard, C., Pierce, N. W., Geoffroy, V., Schaefer, E., Muller, J., Chennen, K., Flori, E., Pelletier, V., Poch, O. et al. (2014). Exome sequencing of bardet-Biedl syndrome patient identifies a null mutation in the BBSome subunit *BBIP1* (*BBS18*). *J. Med. Genet.* **51**, 132-136.
Schulte, R., Talamas, J., Doucet, C. and Hetzer, M. W. (2008). Single bead affinity detection (SINBAD) for the analysis of protein-protein interactions. *PLoS ONE* **3**, e2061.
Seo, S., Baye, L. M., Schulz, N. P., Beck, J. S., Zhang, Q., Slusarski, D. C. and Sheffield, V. C. (2010). BBS6, BBS10, and BBS12 form a complex with CCT/TRiC family chaperonins and mediate BBSome assembly. *Proc. Natl. Acad. Sci. USA* **107**, 1488-1493.
Shaner, N. C., Steinbach, P. A. and Tsien, R. Y. (2005). A guide to choosing fluorescent proteins. *Nat. Methods* **2**, 905-909.
Shibata, H., Inuzuka, T., Yoshida, H., Sugiura, H., Wada, I. and Maki, M. (2010). The ALG-2 binding site in Sec31A influences the retention kinetics of Sec31A at the endoplasmic reticulum exit sites as revealed by live-cell time-lapse imaging. *Biosci. Biotech. Biochem.* **74**, 1819-1826.
Sung, C.-H. and Leroux, M. R. (2013). The roles of evolutionarily conserved functional modules in cilia-related trafficking. *Nat. Cell Biol.* **15**, 1387-1397.
Takahashi, S., Kubo, K., Waguri, S., Yabashi, A., Shin, H.-W., Katoh, Y. and Nakayama, K. (2012). Rab11 regulates exocytosis of recycling vesicles at the plasma membrane. *J. Cell Sci.* **125**, 4049-4057.
Terbush, D. R., Guo, W., Dunkelbarger, S. and Novick, P. (2001). Purification and characterization of yeast exocyst complex. *Meth. Enzymol.* **329**, 100-110.
Vega, I. E. and Hsu, S.-C. (2001). The exocyst complex associates with microtubules to mediate vesicle targeting and neurite outgrowth. *J. Neurosci.* **21**, 3839-3848.
Zhang, Q., Yu, D., Seo, S., Stone, E. M. and Sheffield, V. C. (2012). Intrinsic protein-protein interaction-mediated and chaperonin-assisted sequential assembly of stable Bardet-Biedl syndrome protein complex, the BBSome. *J. Biol. Chem.* **287**, 20625-20635.
Zhou, Y., Hong, W. and Lu, L. (2013). Imaging beads-retained prey assay for rapid and quantitative protein-protein interaction. *PLoS ONE* **8**, e59727.
Zolghadr, K., Mortusewicz, O., Rothbauer, U., Kleinhans, R., Goehler, H., Wanker, E. E., Cardoso, M. C. and Leonhardt, H. (2008). A fluorescent two-hybrid assay for direct visualization of protein interactions in living cells. *Mol. Cell. Proteomics* **7**, 2279-2287.

Journal of Cell Science